Available online at www.sciencedirect.com
ScienceDirect
Journal of Computational Physics 223 (2007) 822–845
JOURNAL OF COMPUTATIONAL PHYSICS
www.elsevier.com/locate/jcp

A relaxation-projection method for compressible flows. Part I: The numerical equation of state for the Euler equations

Richard Saurel *, Erwin Franquet, Eric Daniel, Olivier Le Metayer

Polytech'Marseille, University Institute of France, Université de Provence and SMASH Project UMR CNRS 6595 – IUSTI-INRIA, 5 rue E. Fermi, 13453 Marseille Cedex 13, France

Received 30 September 2005; received in revised form 27 September 2006; accepted 4 October 2006
Available online 27 November 2006

Abstract

A new projection method is developed for the Euler equations to determine the thermodynamic state in computational cells. It consists in the resolution of a mechanical relaxation problem between the various sub-volumes present in a computational cell. These sub-volumes correspond to the ones traveled by the various waves that produce states with different pressures, velocities, densities and temperatures. Contrarily to Godunov type schemes the relaxed state corresponds to mechanical equilibrium only and remains out of thermal equilibrium. The pressure computation with this relaxation process replaces the use of the conventional equation of state (EOS). A simplified relaxation method is also derived and provides a specific EOS (named the Numerical EOS). The use of the Numerical EOS gives a cure to spurious pressure oscillations that appear at contact discontinuities for fluids governed by real gas EOS. It is then extended to the computation of interface problems separating fluids with different EOS (liquid–gas interface for example) with the Euler equations. The resulting method is very robust, accurate, oscillation free and conservative. For the sake of simplicity and efficiency the method is developed in a Lagrange-projection context and is validated over exact solutions. In a companion paper [F. Petitpas, E. Franquet, R. Saurel, A relaxation-projection method for compressible flows. Part II: computation of interfaces and multiphase mixtures with stiff mechanical relaxation. J. Comput. Phys. (submitted for publication)], the method is extended to the numerical approximation of a non-conservative hyperbolic multiphase flow model for interface computation and shock propagation into mixtures.

Keywords: Primitive variables computation; Interfaces; Real gases; Multiphase flows; Riemann problem

0. Introduction

The Godunov method, its extensions and approximate versions, is the most popular method to solve hyperbolic systems of conservation laws. However, inaccuracies and even computational failure appear

* Corresponding author. Tel.: +339 128 8511; fax: +339 128 8322.
E-mail address: Richard.Saurel@polytech.univ-mrs.fr (R. Saurel).

0021-9991/$ - see front matter © 2006 Elsevier Inc. All rights reserved.
doi:10.1016/j.jcp.2006.10.004

when dealing with complicated equations of state and interfaces separating fluids governed by different EOS [1,9,11,18,20]. Most of these inaccuracies do not come from the Riemann problem solution but are related to the use of cell averaged conservative variables used for the pressure computation. Indeed, a computational cell contains several states with different pressures, velocities, densities and temperatures resulting of wave's propagation inside the cell. From these non-equilibrium states, an average state is computed. With conventional methods, it is assumed that this average state can be used for the pressure and temperature computation with the help of the EOS. At this point, the EOS is used with the cell averaged variables. This is the origin of the inaccuracies as the EOS is aimed to relate local thermodynamic variables and not averaged ones. Such a procedure results also in the determination of a single temperature. The computational cell having a finite size and heat conduction being absent of the equations there is no reason that the various temperatures present inside the cell after waves propagation relax to a single equilibrium temperature. It results in pressure and velocity oscillations and even in computational failure when the equation of state is very nonlinear or discontinuous (discontinuous coefficients of the EOS appear at material interfaces).

In other words, in a given cell, the pressure p and if necessary the temperature T are computed with the equations of state $p = p(\rho, e)$ and $T = T(\rho, e)$ with cell averaged density $\langle\rho\rangle$ and internal energy $\langle e\rangle$. It is assumed that the cell pressure and temperature can be obtained as:

$$\langle p\rangle = p(\langle\rho\rangle, \langle e\rangle), \quad \langle T\rangle = T(\langle\rho\rangle, \langle e\rangle) \tag{0.1}$$

even if the equations of state are nonlinear functions of density and internal energy. As the equations of state are valid only with local variables ($p = p(\rho, e)$, $T = T(\rho, e)$) and the cell contains several temperatures and densities, the use of (0.1) is illicit.

In the present paper, we propose a new method to obtain the cell pressure by solving a relaxation system where the equilibrium state corresponds to mechanical equilibrium only. With the new projection method the computational cell is divided in sub-volumes corresponding to the distance covered by the various waves during the time step. For example, with a Lagrangian method, only two waves enter a computational cell leading to three separate sub-volumes. These sub-volumes contain different states regarding pressure, velocity, density and temperature. Instead of averaging the conservative variables present in the various sub-volumes, a mechanical relaxation system is built that expresses the various sub-volume interactions. The asymptotic solution is determined as a set of algebraic relations. Solution of this system provides the cell pressure and velocity at mechanical equilibrium while the sub-volumes states remain out of thermal equilibrium. The relaxed state, determined at the end of each time step for each computational cell prevents the use of the EOS (0.1) with averaged variables.

This method is demonstrated to be equivalent to the Godunov method when used with the ideal gas and stiffened gas equations of state. In the context of more complicated equations of state (Mie–Grüneisen for example) the method is shown to converge to the exact solution with oscillation free solutions while the Godunov method produces spurious oscillations that possibly result in computational failure.

The relaxation method being computationally expensive, an approximate version is derived. It results in a numerical EOS of explicit form that replaces Eq. (0.1). It is first developed in the context of the Mie-Gruneisen EOS for a single fluid. Second, it is extended to the computation of interface problems when equations of state parameters are discontinuous. With the numerical EOS, conservative and oscillation free results are obtained. The method is robust and of comparable computational cost as conventional methods used for the Euler equations. Extension of this method to the numerical approximation of a non-conservative hyperbolic multiphase flow model is the aim of a companion paper [12].

The paper is organized as follows.

The relaxation-projection method is simplified when the number of sub volumes inside a computational cell is limited. We adopt a Lagrange-projection method in order to only have three sub-volumes. The basis of Lagrange-projection methods with conventional Godunov averages is recalled in Section 1.

In Section 2, the relaxation-projection method is presented. First, the relaxation system is built. It resembles to pressure and velocity relaxation systems used for multiphase flows [14,16]. Second, an approximate integration of the relaxation system is done resulting in an algebraic nonlinear system. Its resolution provides the cell pressure.

The method is compared to the Godunov average in Section 3. A demonstration is given showing that both methods identify when the ideal gas and stiffened gas EOS are used. It also explains why the Godunov method is inaccurate for more complex EOS.

The method being computationally expensive, a simplified version is derived in Section 4. Under mild assumptions, the asymptotic solution of the relaxation system is provided by some kind of EOS (the numerical EOS) that allows the cell pressure computation as a function of the same variables as Eq. (0.1) complemented by the distances (or volumes) covered by the various waves entering the computational cell. The numerical EOS is first developed for the Mie-Gruneisen EOS and then extended in Section 5 to the computation of interface problems where the EOS parameters are discontinuous. Computational results are validated against exact solutions and show a perfect agreement.

1. Basis of Lagrange-projection methods with conventional averages

The projection-relaxation method developed in this paper is based on the asymptotic solution of a mechanical relaxation problem involving the various sub-volumes present in a computational cell. These sub-volumes correspond to the propagation distances of the various waves during a time step. This method is easier to implement and to present in the context of Lagrange-projection methods. In this case a computational cell is divided in three sub-volumes defined by the two entering acoustic or shock waves. The use of a conventional Eulerian method leads to a variable number of sub-volumes ranging from 1 to 7 that complicates both presentation and implementation. Other arguments in favor of this strategy are related, for example, to sonic points that do not require specific treatment with Lagrange-projection methods.

Thus, the basis of Lagrange-projection methods is recalled in one space dimension. The system of partial differential equations to solve is:

$$\frac{\partial U}{\partial t}+\frac{\partial F(U)}{\partial x}=0 \tag{1.1}$$

with $U=(\rho,\rho u,\rho E)^{\mathrm{T}}$ and $F(U)=(\rho u,\rho u^2+p,(\rho\ E+p)u)^{\mathrm{T}}$. The total energy is defined by $E=e+\frac{1}{2}u^2$ and the pressure is given, for example, by the stiffened gas (SG) EOS:

$$p=(\gamma-1)\rho e-\gamma p_\infty. \tag{1.2}$$

In these equations, ρ is the density, u is the velocity, p is the pressure, e is the internal energy, γ is the polytropic coefficient and p_∞ is a constant reference pressure.

The first step of this method consists in the solution of the Euler equations in Lagrange coordinates. The second step corresponds to the projection of the solution on a fixed (Eulerian) mesh.

1.1. Lagrange step

Let us consider a computational cell $C_i(t)=[x_{i-1/2}(t),x_{i+1/2}(t)]$. During a time step, the cell boundaries move with constant velocities:

$$x_{i\pm1/2}^{n+1}=x_{i\pm1/2}^{n}+\Delta t u_{i\pm1/2}^{*}, \tag{1.3}$$

where $\Delta t=t^{n+1}-t^n$ is the time step and $u_{i\pm1/2}^{*}$ is the velocity obtained from the Riemann problem solution at the considered cell boundary.

The integration of the Euler equations over time varying cells reads:

$$\int_{t^n}^{t^{n+1}}\frac{\mathrm{d}}{\mathrm{d}t}\int_{C_i(t)}U\,\mathrm{d}x\,\mathrm{d}t+\int_{t^n}^{t^{n+1}}\int_{S_i(t)}(F(U)-u^*U)\,\mathrm{d}S\,\mathrm{d}t=0, \tag{1.4}$$

where $S_i(t)$ represents the contour of the control volume $C_i(t)$. In 1D and under CFL restriction formula (1.4) becomes:

$$U_i^{n+1}=[\Delta x_i^n U_i^n-\Delta t(F^*_{\mathrm{lag}_{i+1/2}}-F^*_{\mathrm{lag}_{i-1/2}})]/\Delta x_i^{n+1}, \tag{1.5}$$

where $\Delta x_i=x_{i+1/2}-x_{i-1/2}$ and $F_{\mathrm{lag}}=F(U)-uU=(0,p,pu)^{\mathrm{T}}$.

Formula (1.5) corresponds to a first order time and space approximation of the Euler equations. By using piecewise linear reconstruction, there is no difficulty to extend the Lagrange step to second order, following the MUSCL algorithm [22].

The vector U_i^{n+1} being determined it is now projected onto the Eulerian grid.

1.2. Projection onto the Eulerian grid

The vector of conservative variables being determined on the Lagrangian mesh, the solution can be projected onto the Eulerian mesh. In Fig. 1, the boundaries trajectories of the Lagrangian cells are shown in dashed lines. In the same graph three levels of conservative variables (grey areas) are shown: at the left of the considered Lagrangian cell, at the right of the Lagrangian cell and in the cell. The Eulerian cells are filled by three flow states, present in segments L_1, L_2 and L_3.

The solution in the Eulerian cell is thus obtained by a simple geometrical projection of the conservative variables:

$$U_{i,\mathrm{e}}^{n+1} = \frac{1}{\Delta x_i}[L_1 U_{i-1}^{n+1} + L_2 U_i^{n+1} + L_3 U_{i+1}^{n+1}], \tag{1.6}$$

where the subscript 'e' in $U_{i,\mathrm{e}}^{n+1}$ denotes the solution in the Eulerian grid. The segments' lengths are given by:

$$L_1 = \max(0, u^*_{i-1/2})\Delta t, \quad L_3 = -\min(0, u^*_{i+1/2})\Delta t, \quad L_2 = \Delta x_i - L_1 - L_3.$$

By introducing normalized length (or volume fractions) $\beta_j = \frac{L_j}{\Delta x_i}$, $j = 1, \ldots, 3$. Formula (1.6) becomes:

$$U_{i,\mathrm{e}}^{n+1} = \sum_{j=1}^{3} \beta_j U_j^{n+1} \tag{1.7}$$

with $U_1^{n+1} = U_{i-1}^{n+1}$, $U_2^{n+1} = U_i^{n+1}$, $U_3^{n+1} = U_{i+1}^{n+1}$.

To proceed to the next time step the pressure computation is necessary. The internal energy is obtained from $(\rho e)_{i,\mathrm{e}}^{n+1} = (\rho E)_{i,\mathrm{e}}^{n+1} - \frac{(\rho u)_{i,\mathrm{e}}^{n+1^2}}{2(\rho)_{i,\mathrm{e}}^{n+1}}$ and the pressure is computed by the EOS (1.2).

There is no difficulty to reduce the numerical diffusion of the projection step (1.6) by using piecewise-linear reconstruction [21], instead of the piecewise constant functions shown in Fig. 1.

There are some advantages with Lagrange-projection methods:

- The Riemann problem is much simpler compared to conventional Eulerian methods. Indeed, only the pressure and the velocity are to be known at the cell boundaries.
- The rarefaction waves and the possible sonic points do not require any special treatment. This advantage will be of major importance when multiphase flows will be considered.

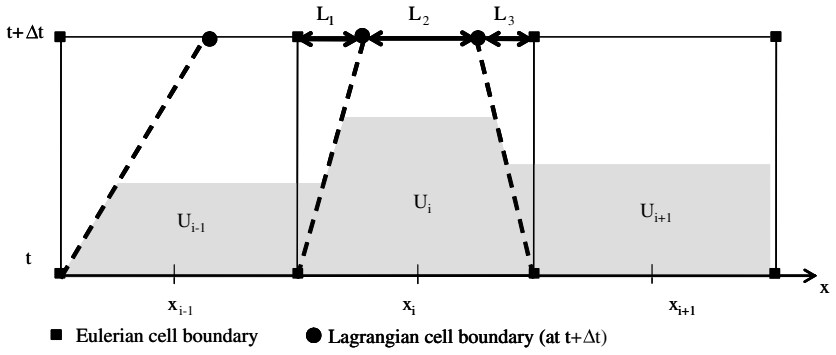

Fig. 1. Schematic view of the different Lagrangian and Eulerian cells. The grey areas correspond to three levels of conservative variables, in the cell and its neighbors.

There are obviously some drawbacks. The most important is related to the extension to non-structured meshes. We restrict here to applications that can be solved with Cartesian meshes.

1.3. Examples

Lagrange-projection methods are quite unusual compared to Eulerian methods. It is thus interesting to report the behavior of a second order Lagrange-projection method on a simple but relevant test case. Let us consider a 1 m length shock tube, containing two chambers separated by an interface at location $x = 0.5$ m. Each chamber is filled with air ($\gamma = 1.4$, $p_\infty = 0$ Pa). At the left of the interface, the initial pressure is equal to 2×10^5 Pa and the initial density is equal to 2 kg/m^3. At the right, the pressure is equal to 10^5 Pa, and the density is equal to 1 kg/m^3. The fluid is initially at rest in both chambers. The solution is shown at time $t = 1.01$ ms. A mesh involving 100 cells is used.

The solution of the Lagrange-projection method with piecewise linear reconstruction and Superbee limiter in both Lagrange and projection steps is used. A 2-shocks Riemann solver [19] is used. In Fig. 2, the density, pressure and velocity profiles are shown with symbols and compared to the exact solution with lines.

The Lagrange-projection method presented in this section provides results of comparable accuracy to second order Eulerian Godunov type schemes. The cell pressure is computed by the means of the EOS (1.2) with the cell averages as arguments, provided by Formula (1.7). When dealing with complex EOS, this procedure

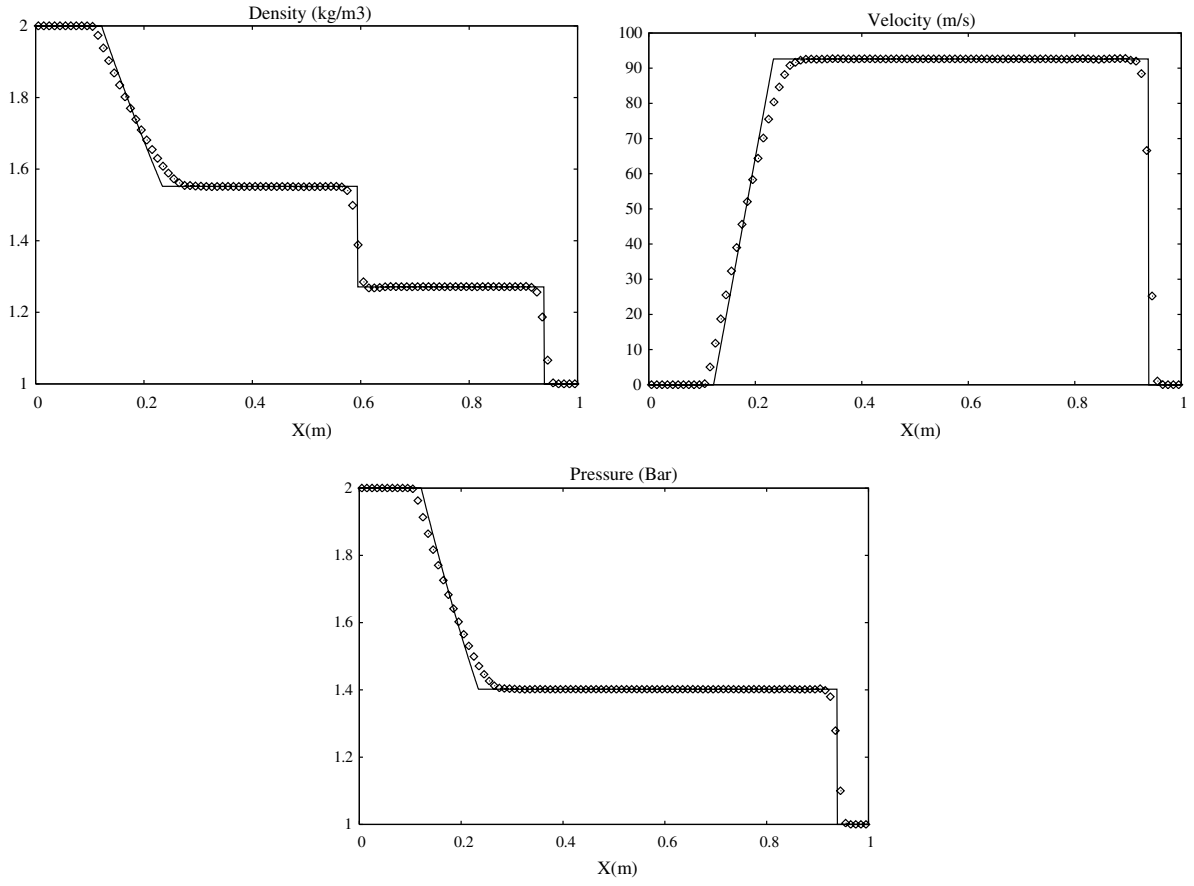

Fig. 2. Shock tube problem. Comparison of the Lagrange-projection with Superbee limiter (symbols) and the exact solution (solid lines). A mesh involving 100 cells is used and the solution is shown at time $t = 1.01$ ms. A comparable accuracy to second order Eulerian Godunov schemes is reported.

based on the EOS with cell averages produces pressure and velocity oscillations at contact discontinuities. This is not specific of the Lagrange-projection method nor of the Riemann solver. It occurs with any type of numerical scheme as soon as the EOS is used with cell averages as arguments. For example, let us consider a fluid that obeys a Mie–Grüneisen type EOS. More precisely, we use the Cochran–Chan EOS [3] presented under Mie–Grüneisen form to describe liquid nitromethane:

$$p(\rho, e) = \rho\Gamma(e - e_k(\rho)) + p_k(\rho),$$

with

$$e_k(\rho) = \frac{A_1}{\rho_{\text{ref}}(E_1 - 1)}\left(\frac{\rho}{\rho_{\text{ref}}}\right)^{E_1 - 1} - \frac{A_2}{\rho_{\text{ref}}(E_2 - 1)}\left(\frac{\rho}{\rho_{\text{ref}}}\right)^{E_2 - 1},$$
$$p_k(\rho) = A_1\left(\frac{\rho}{\rho_{\text{ref}}}\right)^{E_1} - A_2\left(\frac{\rho}{\rho_{\text{ref}}}\right)^{E_2}.$$

The data used in the present simulations are: $\Gamma = 1.19$, $\rho_{\text{ref}} = 1134\ \text{kg/m}^3$, $A_1 = 0.819181 \times 10^9$ Pa, $A_2 = 1.50835 \times 10^9$ Pa, $E_1 = 4.52969$ and $E_2 = 1.42144$.

We consider the advection of a density discontinuity in a uniform flow moving at 1000 m/s in a uniform pressure field. The pressure is taken equal to 2×10^{10} Pa, characteristic of detonation pressure level. The discontinuity is initially located at $x = 0.5$ m and separates two states of density $\rho = 1134\ \text{kg/m}^3$ on the left and lower density ($\rho = 500\ \text{kg/m}^3$) on the right. The Godunov scheme (Eulerian version) is used with an exact Riemann solver. The Riemann solver is detailed in [13] and improved in [12]. The results are shown at time $t = 40$ μs in Fig. 3. The mesh involves 500 cells.

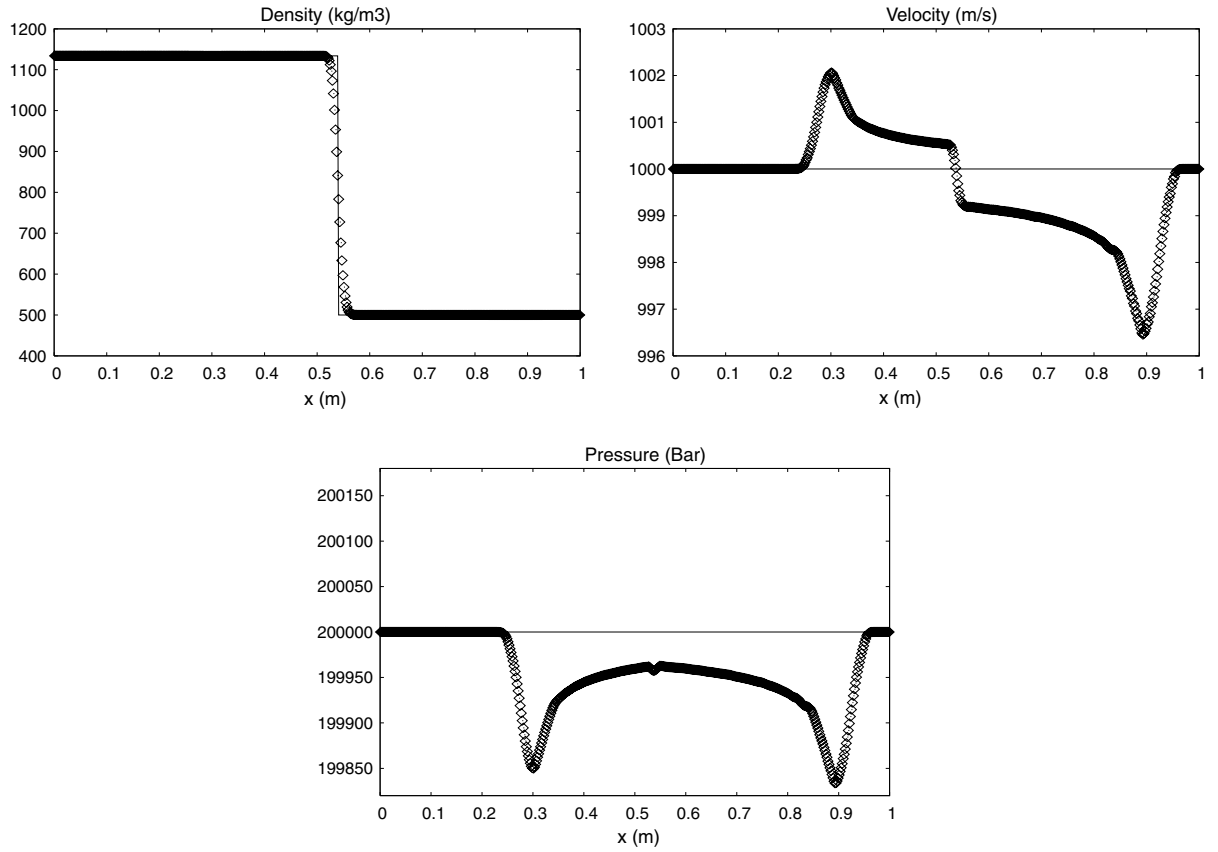

Fig. 3. Advection of a density discontinuity with the Cochran–Chan EOS. The solution obtained with the Godunov scheme is shown with symbols and the exact solution is shown with solid lines. Spurious oscillations appear.

Unphysical oscillations appear at the contact discontinuity and propagate in the flow. It is the reason why a new relaxation-projection method is developed to replace the conventional procedure based on cell averages. With this new method, the cell pressure is determined by solving a relaxation system involving the various non-equilibrium sub-volumes present in a computational cell. These sub-volumes correspond to the ones traveled by the incoming waves into the cell.

2. A relaxation-projection method to compute the cell pressure

The relaxation-projection method presented hereafter is developed to cure some anomalous behavior of Godunov type methods in the context of the Euler equations when dealing with complex EOS.

The method requires that each wave be treated as a discontinuity. Iterative 2-shocks Riemann solver [19] or non-iterative approximate solvers [7] are possible candidates. Such approximation has no serious consequences on rarefaction waves computation, as shown in the previous example of Fig. 2, where a 2-shocks Riemann solver was used. A schematic view of the wave's propagation into a Lagrangian cell is shown in Fig. 4.

Only two waves enter the Lagrangian cell:

- $S^{+}_{i-1/2}$ represents a right-facing shock or rarefaction wave.
- $S^{-}_{i+1/2}$ represents a left-facing shock or rarefaction wave.

The cell volume at time t^{n+1} is given by: $\Delta x_i^{n+1} = \Delta x_i^n + \Delta t(u^*_{i+1/2} - u^*_{i-1/2})$.

This volume can be split into three sub-volumes, each of them containing the fluid in three different states: $L_1 = \Delta t(S^{+}_{i-1/2} - u^*_{i-1/2})$, $L_3 = \Delta t(u^*_{i+1/2} - S^{-}_{i+1/2})$; $L_2 = \Delta x_i^{n+1} - L_1 - L_3$.

As previously, volume fractions can be defined: $\beta_j = \frac{L_j}{\Delta x_i^{n+1}}$, $j = 1, \ldots, 3$.

The cell average state is obtained by:

$$U_i^{n+1} = \sum_{j=1}^{3} \beta_j U_j^* \tag{2.1}$$

with $U_1^* = U^*_{R,i-1/2}$, $U_2^* = U_i^n$, $U_3^* = U^*_{\mathrm{L},i+1/2}$, where indexes L and R refer to the left- and right- states in the Riemann problem.

When dealing with conservation laws it is quite straightforward to show the equivalence of Formulae (2.1) and (1.5). Formula (1.5) is often preferred because of its ability to accept larger time steps. However, with both formulas, computation of the pressure induces errors. Indeed, as mentioned in Section 0, the EOS is valid only with local variables, not averaged ones. Here, each sub-volume L_j contains a fluid in a state denoted by U_j^*. All these states correspond to different densities, pressures, velocities and temperatures. Thus, the use of the equation of state with cell averaged variables, $\langle p\rangle = p(\langle\rho\rangle, \langle e\rangle)$, $\langle T\rangle = T(\langle\rho\rangle, \langle e\rangle)$, where the cell average density $\langle\rho\rangle$ and internal energy $\langle e\rangle$ are taken from the vector of averaged conservative variables U_i^{n+1}, is illicit. Such approximation is usually accepted but produces important errors, especially when dealing with complex EOS.

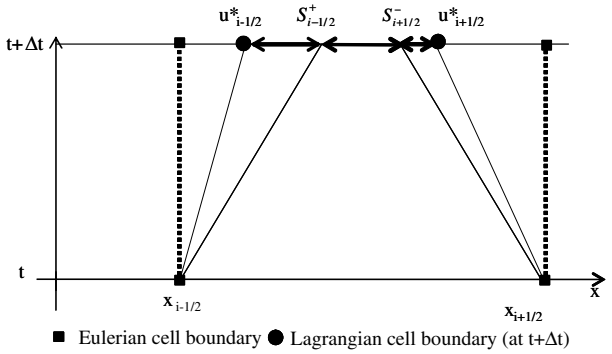

Fig. 4. Schematic view of the waves incoming a Lagrangian cell.

To cure these errors we replace the EOS by a relaxation system connecting the various non-equilibrium states inside the cell. We then determine the equilibrium pressure in the Lagrangian cell as the asymptotic solution of this relaxation system. We present hereafter the relaxation system.

2.1. Relaxation system

The waves have entered the considered Lagrangian cell and each sub-volume L_j contains a fluid in a state different of the one in the direct neighboring sub-volume. All physical variations that make the solution evolve have already been involved in the incoming waves shown in Fig. 3, and the goal is now to determine the cell equilibrium pressure.

As physical variations due to interactions with the neighboring cells are already contained in the current cell, we isolate the cell from the others. The cell now contains three non-equilibrium states in three sub-volumes and interactions occur between these states in the isolated cell.

For the sake of simplicity, let us consider two sub-volumes only inside a cell. Consider the situation shown in Fig. 4 and imagine that $S^{+}_{i-1/2}$ is a right-facing shock or rarefaction wave and that $S^{-}_{i+1/2}$ has zero amplitude, and thus produces no variation. Such a situation is shown in Fig. 5.

At the beginning of the relaxation process ($\tau = 0$), two states are present inside the cell separated by a discontinuity corresponding to the incoming wave position. These states correspond to the ones obtained from the Riemann problem solution. The cell being isolated from the neighboring ones, periodic boundary conditions are present on the right and left cell boundaries. From this initial situation, the sub-volumes expand or contract according to their pressure and velocity differentials. The sub-volumes also move inside the cell until they reach pressure and velocity equilibrium when pseudo time τ tends to infinity.

The first issue with the present method consists in the building of the relaxation system that drives the non-equilibrium sub-volumes and states toward mechanical equilibrium.

In each sub-volume, the fluid is governed by the Euler equations. In order to select the appropriate state in each sub-volume j, we introduce a characteristic function X_j:

$$X_j(x,\tau) = \begin{cases} 1 & \text{if } x \text{ belongs to the state } j, \\ 0 & \text{otherwise.} \end{cases}$$

This function obeys the evolution equation:

$$\frac{\partial X_j}{\partial \tau} + \sigma \frac{\partial X_j}{\partial x} = 0, \tag{2.2}$$

where σ represents the *local* interface velocity.

The Euler equations (1.1) are valid for any state of the fluid. Here, this system is completed by a trivial identity ($\frac{\partial 1}{\partial \tau} + \frac{\partial 0}{\partial x} = 0$) that simplifies the presentation of the volume fraction equation. Thus system (1.1) now reads:

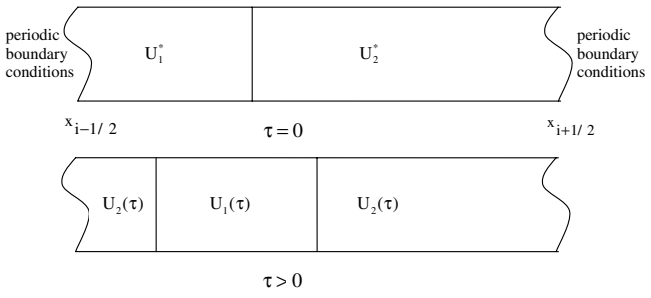

Fig. 5. Schematic view of two non-equilibrium states inside a cell resulting of a single right-facing wave emerging of the left cell boundary. The situation on top corresponds to the one at the end of wave propagation and at the beginning of the relaxation process, at pseudo time $\tau = 0$. The situation at the bottom corresponds to the one during the relaxation process. The volumes of fluids have moved as the states have different velocities and pressures. Periodic boundary conditions are present as the cell is isolated from the others.

$$\frac{\partial U}{\partial \tau}+\frac{\partial F(U)}{\partial x}=0 \tag{2.3}$$

with $U=(1,\rho,\rho u,\rho E)^{\mathrm{T}}$ and $F(U)=(0,\rho u,\rho u^2+p,(\rho E+p)u)^{\mathrm{T}}$.

The average state in each sub volume is obtained by:

– Selecting the corresponding state. This step is achieved by multiplying the Euler equations (2.3) by the characteristic function X_j.
– Integrating over space the selected system.

This method has been developed in the context of multiphase mixtures by Abgrall and Saurel [2], Saurel et al. [17], Chinnayya et al. [4], Le Metayer et al. [10]. In the present context we have to integrate

$$\int_{x_{i-1/2}}^{x_{i+1/2}}\left(\frac{\partial X_j U}{\partial \tau}+\frac{\partial X_j F}{\partial x}\right)\mathrm{d}x=\int_{x_{i-1/2}}^{x_{i+1/2}}(F-\sigma U)\frac{\partial X_j}{\partial x}\,\mathrm{d}x. \tag{2.4}$$

With the previous notations and with the help of the trivial identity, the evolution of the characteristic function is recovered.

The flux divergence vanishes due to the presence of periodic boundary conditions. The system now reduces to:

$$\int_{x_{i-1/2}}^{x_{i+1/2}}\frac{\partial X_j U}{\partial \tau}\,\mathrm{d}x=\int_{x_{i-1/2}}^{x_{i+1/2}}(F-\sigma U)\frac{\partial X_j}{\partial x}\,\mathrm{d}x. \tag{2.5}$$

The terms in the right-hand side of this equation represent the Lagrangian flux:

$$F_{\mathrm{lag}}=F-\sigma U=(-u,0,p,pu)^{\mathrm{T}}.$$

At each interface separating two states the Lagrangian flux is constant, as the interface condition corresponds to constant pressure and velocity. This remark renders possible integration of (2.5). For state 1 it reads:

$$\frac{\partial}{\partial \tau}\int_{x_{i-1/2}}^{x_{i+1/2}}X_1 U\,\mathrm{d}x=F^*_{\mathrm{lag},12}[X_1]_{12}+F^*_{\mathrm{lag},21}[X_1]_{21}. \tag{2.6}$$

The two terms on the right-hand side of (2.6) come from the two interfaces present in the cell. At these interfaces only, the gradient of the characteristic function is non zero. At these locations, two instances are possible:

– State 1 is on the left and state 2 on the right. Such situation corresponds to the flow pattern (12).
– State 2 is on the left and state 1 on the right, corresponding to the flow pattern (21).

For each flow pattern (12) or (21) the Riemann problem is solved and the Lagrangian flux is computed. This Lagrangian flux is constant at the location where $\frac{\partial X_j}{\partial x}\neq 0$, i.e. at the interfaces. Consequently, the product $(F-\sigma U)\frac{\partial X_j}{\partial x}$ is integrated easily. It provides the two terms of Eq. (2.6), where:

– $F^*_{\mathrm{lag},12}$ represents the Lagrangian flux, solution of the Riemann problem with state 1 on the left and state 2 on the right,
– $[X_1]_{12}$ represents the jump of the characteristic function $[X_1]$ with fluid 1 on the left and fluid 2 on the right.

With these notations, it is easily deduced that $[X_1]_{12}=-1$ and $[X_1]_{21}=1$.

Thus, Eq. (2.6) reduces to:

$$\frac{\partial}{\partial \tau}\int_{x_{\mathrm{L}}}^{x_{\mathrm{R}}}U_1\,\mathrm{d}x=F^*_{\mathrm{lag},21}-F^*_{\mathrm{lag},12}, \tag{2.7}$$

where x_{L} and x_{R} represent the left and right boundaries of the sub-volume of state 1.

By defining the state average:

$$\overline{U}_1 = \frac{1}{x_R - x_L}\int_{x_L}^{x_R} U_1 \, dx.$$

Eq. (2.7) becomes:

$$\frac{\partial (x_R - x_L)\overline{U}_1}{\partial \tau} = F^*_{lag,21} - F^*_{lag,12}.$$

Now, dividing this result by $\Delta x = x_{i+1/2} - x_{i-1/2}$ we get:

$$\frac{\partial \beta_1 \overline{U}_1}{\partial \tau} = \frac{1}{\Delta x}(F^*_{lag,21} - F^*_{lag,12}) \tag{2.8}$$

where $\beta_1 = \frac{x_R - x_L}{\Delta x}$ represents the volume fraction of state 1.

System (2.8) corresponds to a relaxation system. In order to determine the relaxation parameters, the Lagrangian flux has to be developed. It is function only of interface pressure and velocity. Explicit expressions for these variables are available from the acoustic solver [6], in the limit of small amplitude waves:

$$\begin{aligned} p^*_{12} &= \frac{Z_2 p_1 + Z_1 p_2}{Z_1 + Z_2} + \frac{Z_1 Z_2}{Z_1 + Z_2}(u_1 - u_2), \\ u^*_{12} &= \frac{Z_1 u_1 + Z_2 u_2}{Z_1 + Z_2} + \frac{p_1 - p_2}{Z_1 + Z_2}, \end{aligned} \tag{2.9}$$

where $Z_j = (\rho c)_j$ represents the acoustic impedance of state j and c_j the corresponding speed of sound. With the help of (2.9), system (2.8) can be expanded to:

$$\begin{aligned} &\frac{\partial \beta_1}{\partial \tau} = \mu(p_1 - p_2), \\ &\frac{\partial \beta_1 \bar{\rho}_1}{\partial \tau} = 0, \\ &\frac{\partial \beta_1 \overline{\rho_1 u_1}}{\partial \tau} = \lambda(u_2 - u_1), \\ &\frac{\partial \beta_1 \overline{\rho_1 E_1}}{\partial \tau} = \lambda u_I (u_1 - u_2) - \mu p_I (p_1 - p_2). \end{aligned} \tag{2.10}$$

With the interface variables:

$$u_I = \frac{Z_1 u_1 + Z_2 u_2}{Z_1 + Z_2} \quad \text{and} \quad p_I = \frac{Z_2 p_1 + Z_1 p_2}{Z_1 + Z_2},$$

and relaxation coefficients:

$$\mu = \frac{2}{\Delta x (Z_1 + Z_2)} \quad \text{and} \quad \lambda = \mu Z_1 Z_2.$$

These relaxation parameters control, respectively, the rates at which pressure and velocity equilibriums are reached. An analogous system is obtained for state 2.

It appears clearly from system (2.10) that conservation is guaranteed, as well as the saturation constraint $\sum_j \beta_j = 1$. As this system relaxes toward a unique pressure and velocity, it can be used for the pressure and velocity computation inside the cell, instead of the use of the EOS with conventional cell averages as arguments. Such computation has to be done at the end of each time step in the limit $\tau \to +\infty$.

Before examining the practical use of such a method, system (2.10) has to be extended to a computational cell involving three sub-volumes. Such extension is done by noting that, in the preceding context of two states, a more convenient form of system (2.10) is available:

$$\frac{\partial \beta_1}{\partial \tau} = \frac{\delta}{Z_1}(p_1 - p_I),$$
$$\frac{\partial \beta_1 \bar{\rho}_1}{\partial \tau} = 0,$$
$$\frac{\partial \beta_1 \overline{\rho_1 u_1}}{\partial \tau} = \delta Z_1 (u_I - u_1),$$
$$\frac{\partial \beta_1 \overline{\rho_1 E_1}}{\partial \tau} = \delta \left(u_I Z_1 (u_I - u_1) - \frac{p_I}{Z_1}(p_1 - p_I) \right),$$

where $\delta = \frac{2}{\Delta x}$.

Therefore, the extension to the case to three states reads:

$$\begin{aligned}
&\frac{\partial \beta_j}{\partial \tau} = \frac{\delta}{Z_j}(p_j - p_I),\\
&\frac{\partial \beta_j \rho_j}{\partial \tau} = 0,\\
&\frac{\partial \beta_j \rho_j u_j}{\partial \tau} = \delta Z_j (u_I - u_j),\\
&\frac{\partial \beta_j \rho_j E_j}{\partial \tau} = \delta \left(u_I Z_j (u_I - u_j) - \frac{p_I}{Z_j}(p_j - p_I) \right)
\end{aligned} \tag{2.11}$$

with $u_I = \frac{Z_1 u_1 + Z_2 u_2 + Z_3 u_3}{Z_1 + Z_2 + Z_3}$ and $p_I = \frac{\frac{p_1}{Z_1} + \frac{p_2}{Z_2} + \frac{p_3}{Z_3}}{\frac{1}{Z_1} + \frac{1}{Z_2} + \frac{1}{Z_3}}$.

The state volume average symbol has been omitted for the sake of conciseness. Again, it appears that system (2.11) guarantees mass, momentum and energy conservation as well as the saturation constraint $\sum_j \beta_j = 1$.

Examine now the entropy inequality. We first write the energy equation under the form:

$$\frac{\partial \beta_j \rho_j E_j}{\partial \tau} = -p_I \frac{\partial \beta_j}{\partial \tau} + u_I \frac{\partial \beta_j \rho_j u_j}{\partial \tau}.$$

By combining this equation with the mass and momentum equations we obtain:

$$\frac{\partial e_j}{\partial \tau} + (u_j - u_I)\frac{\partial u_j}{\partial \tau} + p_I \frac{\partial v_j}{\partial \tau} = 0 \tag{2.12}$$

with $v_j = 1/\rho_j$.

By using the Gibbs identity, we obtain the following evolution equation for the entropy in sub-volume j:

$$T_j \frac{\partial s_j}{\partial \tau} = (u_I - u_j)\frac{\partial u_j}{\partial \tau} + (p_j - p_I)\frac{\partial v_j}{\partial \tau}.$$

The combination of the volume fraction, mass and momentum equations yields:

$$\beta_j \rho_j T_j \frac{\partial s_j}{\partial \tau} = \delta \left(Z_j (u_I - u_j)^2 + \frac{(p_j - p_I)^2}{Z_j} \right). \tag{2.13}$$

It shows that the entropy production in each sub-volume (for each state of the fluid) is positive or null: the total production for the system is therefore null or positive.

This relaxation problem is thus well-posed and can lead to the determination of the pressure and the velocity in the cell in the asymptotic limit $\tau \to +\infty$. Nevertheless, the numerical integration of the ordinary differential equation (2.11) is too much expensive and not necessary since only the asymptotic state is required. In the next paragraph, this asymptotic solution is reached by an approximate integration.

2.2. Integration of the relaxation problem

Let us denote by the superscript 0 all the variables related to the Riemann problem solution in the Lagrangian cell. The relaxed state at mechanical equilibrium will be denoted by the superscript $*$.

2.2.1. Principles of the relaxed state determination

Integration of Eq. (2.12) between these two states reads:

$$\int_0^{+\infty} \frac{\mathrm{d}e_j(\tau)}{\mathrm{d}\tau}\,\mathrm{d}\tau + \int_0^{+\infty} (u_j(\tau) - u_I(\tau))\frac{\mathrm{d}u_j(\tau)}{\mathrm{d}\tau}\,\mathrm{d}\tau + \int_0^{+\infty} p_I(\tau)\frac{\mathrm{d}v_j(\tau)}{\mathrm{d}\tau}\,\mathrm{d}\tau = 0.$$

It can be written as:

$$e_j^* - e_j^0 + \int_{u_j^0}^{u^*} u_j\,\mathrm{d}u_j - \hat{u}_{Ij}\int_{u_j^0}^{u^*}\mathrm{d}u_j + \hat{p}_{Ij}\int_{v_j^0}^{v_j^*}\mathrm{d}v_j = 0.$$

Or, more simply:

$$e_j^* - e_j^0 + \hat{p}_{Ij}(v_j^* - v_j^0) = q_j \tag{2.14}$$

with

$$q_j = \frac{1}{2}(u^* - u_j^0)(2\hat{u}_{Ij} - (u^* + u_j^0)),$$

$$\hat{p}_{Ij} = \frac{1}{v_j^* - v_j^0}\int_0^{+\infty} p_I\frac{\mathrm{d}v_j}{\mathrm{d}\tau}\,\mathrm{d}\tau \quad \text{and} \quad \hat{u}_{Ij} = \frac{1}{u^* - u_j^0}\int_0^{+\infty} u_I\frac{\mathrm{d}u_j}{\mathrm{d}\tau}\,\mathrm{d}\tau.$$

In these equations, $\hat{p}_{Ij}$ and $\hat{u}_{Ij}$ denote the averages during the relaxation process of the interface pressure and velocity of state j. The velocity at relaxed state is denoted by u^*.

These averaged interface variables have to be determined but we first suppose that their expressions are known in order to present the solution procedure. Their determination will be secondly examined.

The solution procedure starts with the mass conservation of the mixture:

$$\rho^* = \sum_j \beta_j^*\rho_j^* = \sum_j \beta_j^0\rho_j^0 = \rho^0 = \rho. \tag{2.15}$$

The mass equation of each sub-volume implies: $\beta_j^*\rho_j^* = \beta_j^0\rho_j^0$.

That is to say:

$$Y_j^* = \frac{\beta_j^*\rho_j^*}{\rho^*} = \frac{\beta_j^0\rho_j^0}{\rho^0} = Y_j^0 = Y_j. \tag{2.16}$$

The momentum conservation of the mixture reads: $\sum_j \beta_j^*\rho_j^*u_j^* = \sum_j \beta_j^0\rho_j^0u_j^0$.

At relaxed state we have $u_j^* = u^*$. The mixture momentum equation becomes:

$$u^* = \frac{\sum_j \beta_j^0\rho_j^0u_j^0}{\sum_j \beta_j^*\rho_j^*}.$$

It implies the relaxed velocity expression:

$$u^* = \sum_j Y_j u_j^0. \tag{2.17}$$

The determination of the relaxed pressure requires the use of the EOS $e = e(v,p)$. The EOS is used to relate only thermodynamic variables of a given state, not the cell average ones.

For a given cell, as $\hat{p}_{Ij}$ and $\hat{u}_{Ij}$ are supposed known expressions, p^* and the v_j^* $(j = 1,2,3)$ form a set of four unknowns. Relation (2.14) then provides three equations that may be written as:

$$e_j^*(v_j^*, p^*) - e_j^0 + \hat{p}_{Ij}(v_j^* - v_j^0) = q_j. \tag{2.18}$$

The last equation to close the system is obtained by the saturation constraint: $\sum_j \beta_j = 1$, that can be written as:

$$\sum_j m_j v_j(p^*) - 1 = 0 \tag{2.19}$$

with $m_j = \beta_j \rho_j$ the mass in each sub-volume (which is constant during the relaxation process).

The three equations (2.18), completed by Eq. (2.19), form a nonlinear system of four equations for four unknowns $(v_1^*, v_2^*, v_3^*, p^*)$ which is solved by a Newton–Raphson method. The iterative process depending only on the pressure p^*, a simple numerical procedure is easily derived. Let us now examine the possible ways to determine the functions $\hat{p}_{Ij}$ and $\hat{u}_{Ij}$ that realize the closure of (2.14).

2.2.2. Estimates of the interface variables averages

The interface variables averages $\hat{u}_{Ij}$ and $\hat{p}_{Ij}$ have to be determined. As a guideline, the choice of these variables must fulfill energy conservation and entropy inequality.

2.2.2.1. Energy conservation. By grouping internal and kinetic energies, Eq. (2.14) reads:

$$E_j^* - E_j^0 + \hat{p}_{Ij}(v_j^* - v_j^0) = (u^* - u_j^0)\hat{u}_{Ij},$$

and the summation over all sub-volumes reads:

$$\sum_j Y_j E_j^* - \sum_j Y_j E_j^0 + \sum_j \hat{p}_{Ij} Y_j (v_j^* - v_j^0) = \sum_j Y_j \hat{u}_{Ij}(u^* - u_j^0). \tag{2.20}$$

Moreover, the total energy of the mixture is defined by $E = \sum_j Y_j E_j$ and the conservation of the energy implies $E^* - E^0 = 0$. That immediately imposes a constraint on Eq. (2.20) in order to guarantee energy conservation:

$$\sum_j Y_j[-\hat{p}_{Ij}(v_j^* - v_j^0) + \hat{u}_{Ij}(u^* - u_j^0)] = 0. \tag{2.21}$$

Thanks to the saturation constraint $\sum_j \beta_j = 1$ which can be written as $\sum_j \rho Y_j/\rho_j = 1$, we have:

$$\sum_j Y_j/\rho_j = 1/\rho, \quad \text{or} \quad \sum_j Y_j v_j = v. \tag{2.22}$$

The mixture mass conservation (2.15) implies $v^* = v^0$.

With the help of relation (2.17) a sufficient condition appears in order that (2.21) be satisfied: if $\hat{u}_{Ij}$ and $\hat{p}_{Ij}$ do not depend on j, then the energy conservation is guaranteed. It consists in an important simplification but a little restriction regarding the choice of these variables. So, another constraint is considered.

2.2.2.2. Entropy inequality. The use of the second law of thermodynamics is rendered easy if it is assumed that the evolutions of all the variables are infinitesimal. Thus, Eq. (2.14) becomes:

$$\Delta e_j + (u_j - \hat{u}_I)\Delta u_j + \hat{p}_I \Delta v_j = 0, \tag{2.23}$$

where symbol Δ represents a small perturbation and the interface variables averages $\hat{u}_I$ and $\hat{p}_I$ are assumed independent on j.

By using the Gibbs identity, the entropy variation reads:

$$T_j \Delta s_j = (p_j - \hat{p}_I)\Delta v_j + (\hat{u}_I - u_j)\Delta u_j. \tag{2.24}$$

The sign of this variation must be analyzed. To do this, Δv_j has to be expressed along the thermodynamic path corresponding to (2.23). By expanding this relation:

$$\left.\frac{\partial e_j}{\partial p_j}\right|_{v_j} \Delta p_j + \left(\hat{p}_I + \left.\frac{\partial e_j}{\partial v_j}\right|_{p_j}\right)\Delta v_j = (\hat{u}_I - u_j)\Delta u_j,$$

and reminding that $\frac{\partial e_j}{\partial v_j}|_{p_j} = c_j^2/(v_j\Gamma_j) - p_j$ and $\frac{\partial e_j}{\partial p_j}|_{v_j} = v_j/\Gamma_j$ we obtain:

$$\Delta v_j = \frac{(\hat{u}_I - u_j)\Delta u_j - \frac{v_j}{\Gamma_j}\Delta p_j}{\left(\hat{p}_I - p_j + \frac{c_j^2}{v_j\Gamma_j}\right)}, \tag{2.25}$$

where Γ_j is the Grüneisen coefficient and c_j^2 is the square speed of sound.

By inserting this result in (2.24) we get:

$$T_j\Delta s_j = \frac{v_j}{\Gamma_j}\frac{\frac{c_j^2}{v_j^2}(\hat{u}_I - u_j)\Delta u_j - (p_j - \hat{p}_I)\Delta p_j}{\left(\hat{p}_I - p_j + \frac{c_j^2}{v_j\Gamma_j}\right)}.$$

We now use the definition of the polytropic coefficient ($\gamma = \frac{\rho c^2}{p}$), and obtain:

$$T_j\Delta s_j = \frac{\gamma_j}{\Gamma_j}\frac{Z_j^2(\hat{u}_I - u_j)\Delta u_j - (p_j - \hat{p}_I)\Delta p_j}{\left(\hat{Z}_{Ij}^2 + Z_j^2\left(\frac{\gamma_j}{\Gamma_j} - 1\right)\right)} \tag{2.26}$$

with $Z = \rho c$ and $\hat{c}_{Ij}^2 = \gamma_j\hat{p}_I v_j$.

Integration of this relation between state '0' and state '*', by assuming small variations around the initial state $(T_j^0, v_j^0, p_j^0, u_j^0)$, leads to:

$$T_j^0(s_j^* - s_j^0) = \frac{1}{2}\frac{\gamma_j}{\Gamma_j}\frac{Z_j^{0^2}(u^* - u_j^0)(2\hat{u}_I - (u^* + u_j^0)) + (p^* - p_j^0)(2\hat{p}_I - (p^* + p_j^0))}{\left(\hat{Z}_{Ij}^2 + Z_j^{0^2}\left(\frac{\gamma_j}{\Gamma_j} - 1\right)\right)}. \tag{2.27}$$

A sufficient condition in order that $(s_j^* - s_j^0) > 0$ appears:

$$\text{If } \hat{p}_I = p^* \quad \text{and} \quad \hat{u}_I = u^*\left(\text{leading to } q_j = \frac{1}{2}(u^* - u_j^0)^2\right), \tag{2.28}$$

the entropy inequality is fulfilled.

This choice is not unique, but it guarantees energy conservation and fulfils the second law of thermodynamics. These simple estimates are retained in the following and achieve closure of system (2.18), (2.19).

3. Comparison with the Godunov method

The relaxation method based on (2.19), (2.20) is expected to provide results very closed to the ones of the Godunov method. Indeed, it is possible to show that both methods are identical when the ideal gas or stiffened gas EOS are used. However, important differences appear in the computation of contact discontinuities when dealing with complex EOS. The new method is shown to provide oscillation free solutions while the Godunov method exhibits spurious oscillations that may result in computational failure.

These differences are demonstrated with both theoretical arguments and numerical experiments. Let us first demonstrate that the two methods merge in the context of the stiffened gas EOS.

3.1. Stiffened gas EOS

The stiffened gas EOS given by relation (1.2) is considered. With this EOS, it is possible to show that the new method is identical to the Godunov one.

Let us sum relation (2.14) over all the sub-volumes:

$$\sum_j Y_j e_j^* - \sum_j Y_j e_j^0 + \sum_j \hat{p}_I (Y_j v_j^* - Y_j v_j^0) = \sum_j \hat{u}_I Y_j (u^* - u_j^0) - \frac{1}{2}\left(u^{*^2} - \sum_j Y_j u_j^{0^2} \right).$$

With the help of the EOS, $e_j = \frac{(p_j + \gamma_j p_{\infty j}) v_j}{\gamma_j - 1}$ we have:

$$\frac{1}{\rho}\left\{ \sum_j \beta_j^* \frac{p_j^*}{\gamma_j - 1} + \sum_j \beta_j^* \frac{\gamma_j p_{\infty j}}{\gamma_j - 1} \right\} = \sum_j Y_j e_j^0 + \frac{1}{2}\sum_j Y_j u_j^{0^2} - \frac{1}{2} u^{*^2} + \sum_j Y_j [-\hat{p}_I (v_j^* - v_j^0) + \hat{u}_I (u^* - u_j^0)].$$

The state denoted by superscript $*$ is the relaxed one in which pressures and velocities are equals in all sub-volumes. Thus:

$$p^* \left\{ \sum_j \frac{\beta_j^*}{\gamma_j - 1} \right\} = \rho \left\{ E^0 - \frac{1}{2} u^{*^2} + \sum_j Y_j [-\hat{p}_I (v_j^* - v_j^0) + \hat{u}_I (u^* - u_j^0)] \right\} - \sum_j \beta_j^* \frac{\gamma_j p_{\infty j}}{\gamma_j - 1}. \tag{3.1}$$

In the present single phase flow context we have: $\gamma_j = \gamma$ and $p_{\infty j} = p_\infty \ \forall j$.
Thus, Formula (3.1) becomes:

$$p^* = \rho(\gamma - 1)\left\{ E^0 - \frac{1}{2} u^{*^2} + \sum_j Y_j [-\hat{p}_I (v_j^* - v_j^0) + \hat{u}_I (u^* - u_j^0)] \right\} - \gamma p_\infty.$$

The estimates for $\hat{p}_I$ and $\hat{u}_I$ with (2.28) are such that (2.21) is fulfilled. The last equation thus reduces to:

$$p^* = \rho(\gamma - 1)\left\{ E^0 - \frac{1}{2} u^{*^2} \right\} - \gamma p_\infty. \tag{3.2}$$

It is quite interesting to compare this formula with the one obtained with the Godunov scheme. In this case, the pressure is directly computed from the internal energy obtained from the conservative variables according to:

$$(\rho e)_i^{n+1} = (\rho E)_i^{n+1} - \frac{1}{2} \frac{[(\rho u)_i^{n+1}]^2}{(\rho)_i^{n+1}}.$$

The use of the stiffened Gas EOS leads to:

$$p^* = (\gamma - 1)\left\{ (\rho E)_i^{n+1} - \frac{1}{2} \frac{[(\rho u)_i^{n+1}]^2}{(\rho)_i^{n+1}} \right\} - \gamma p_\infty = \rho(\gamma - 1)\left\{ E^0 - \frac{1}{2} u^{*^2} \right\} - \gamma p_\infty.$$

That is exactly the same relation as (3.2). Consequently, the new projection method is equivalent to the Godunov method. Nevertheless, this result depends on the EOS. For more general EOS, this observation is no longer valid.

3.2. More general EOS

Let us consider the example of the Mie–Grünesein (MG) EOS: $p = (\gamma - 1)\rho e - \gamma p_\infty(\rho)$.
The analysis has to be reconsidered from Eq. (3.1) because p_∞ is now depending on the density. As the flow is single phase, we still have $\gamma_j = \gamma \ \forall j$. Eq. (3.1) then becomes:

$$p^* = \rho(\gamma - 1)\left\{ E^0 - \frac{1}{2} u^{*^2} \right\} - \gamma \sum_j \beta_j^* p_{\infty j}(\rho_j^*). \tag{3.3}$$

With the Godunov scheme, the pressure is computed by:

$$p^* = \rho(\gamma - 1)\left\{ E^0 - \frac{1}{2} u^{*^2} \right\} - \gamma p_\infty(\rho). \tag{3.4}$$

The methods are now different and it is necessary to determine which method is in error. A direct evaluation of p^* given by (3.3) is not easy because the functions β_j^* and ρ_j^* vary between the state '0' and the relaxed state '*'. However, there is a case where this calculation is trivial. This case corresponds to a contact discontinuity moving in a uniform pressure and velocity flow. In this context the pressure at the end of the time step, must be equal to the initial pressure.

Let us examine formula (3.3): $p^* = \rho(\gamma-1)\{e^0 + \frac{1}{2}\sum_j Y_j u_j^{0^2} - \frac{1}{2}u^{*^2}\} - \gamma\sum_j \beta_j^* p_{\infty j}(\rho_j^*)$.

As the flow velocity is uniform it reduces to: $p^* = \rho(\gamma-1)e^0 - \gamma\sum_j \beta_j^* p_{\infty j}(\rho_j^*)$.

By using the definition of the mixture internal energy, $\rho e^0 = \sum_j \beta_j^0 \rho_j^0 e_j^0$, we obtain:

$$p^* = \sum_j \beta_j^0 \rho_j^0 (\gamma-1) e_j^0 - \sum_j \beta_j^* \gamma p_{\infty j}(\rho_j^*).$$

All pressures p_j^0 and velocities u_j^0 are the same for the uniform flow under interest. Thus, there is no mechanism able to produce a change in the sub-volume fractions β_j or in the densities ρ_j.

That is to say:

$$p^* = \sum_j \beta_j^0 p_j^0 + \gamma \sum_j \beta_j^0 (p_{\infty j}(\rho_j^0) - p_{\infty j}(\rho_j^*)).$$

We thus have:

$$p^* = \sum_j \beta_j^0 p_j^0 = p^0. \tag{3.5}$$

The new projection method leads to the correct pressure for this particular case of uniform pressure and velocity flow.

Let us now calculate the pressure with relation (3.4) used in Godunov type methods. The kinetic energies vanish as previously. By using the definition of the mixture internal energy we have:

$$p^* = \sum_j \beta_j^0 \rho_j^0 (\gamma-1) e_j^0 - \gamma p_\infty(\rho).$$

By using the EOS in each sub-volume we get:

$$p^* = \sum_j \beta_j^0 p_j^0 + \gamma \sum_j \beta_j^0 p_{\infty j}(\rho_j^0) - p_\infty(\rho) = p^0 + \gamma \sum_j \beta_j^0 p_{\infty j}(\rho_j^0) - p_\infty(\rho).$$

In order to have a correct evolution of the pressure, it is necessary that $p^* = p^0$. This condition is true if and only if:

$$\sum_j \beta_j^0 p_{\infty j}(\rho_j^0) = p_\infty(\rho) \quad \text{with } \rho = \sum_j \beta_j^0 \rho_j^0. \tag{3.6}$$

This condition is satisfied if and only if $p_\infty(\rho)$ is a linear function of the density, or if the densities ρ_j^0 are all equal. In the general case, $p_\infty(\rho)$ is a nonlinear function and the density is discontinuous at contact surfaces. It implies that the Godunov scheme cannot preserve a contact discontinuity moving in a uniform flow when the MG EOS is used. This result is also true for any EOS involving nonlinear density or energy contributions.

3.3. Summary of the relaxation-projection method

The new method is able to solve contact discontinuities with real gas EOS with oscillation free solutions. The relaxation procedure allows the pressure computation in both Lagrangian and Eulerian cells from the three non-equilibrium states resulting of the wave's propagation.

When the computation is purely Lagrangian, the relaxed velocity is given by (2.17), the average density is given by (2.15) and the relaxed pressure is obtained by the resolution of System (2.18), (2.19).

When the solution strategy is based on Eulerian projection, there is no need to compute the Lagrangian cell pressure. The Lagrangian conservative variables vector is projected in a fixed (Eulerian) grid. The situation is

depicted in Fig. 1: Three states (actually 1 up to 3 states), defined by three Lagrangian cells, can overlap a given Eulerian cell. From these three states the determination of a unique state into the Eulerian cell is obtained by relation (1.7). The relaxed pressure is computed by solving System (2.18), (2.19).

At the end of this time step, both conservative and primitive variable vectors are known in Eulerian cells. Such computation preserves interface conditions.

Let us summarize the present algorithm:

- At the initial time, the conservative variable vector $U = (\rho, \rho u, \rho E)^{\mathrm{T}}$ is defined in all Eulerian cells. The Lagrangian and Eulerian cells are merged at the initial time.
- At each Lagrangian cell boundary, the solution of Riemann problems is solved with an iterative 2-shocks or approximate HLLC solver [19] with Davis [5] wave's speeds estimates. The Riemann problem solution provides the various wave speeds and states. From their knowledge, the three sub-volumes and states are obtained in the Lagrangian cell.
- The conservative variable vector is updated with (1.5). The Lagrangian cell relaxed pressure is obtained by solving (2.19), (2.20). Pressure computation is not necessary if the solution is immediately projected onto the Eulerian grid.
- The motion of the Lagrangian cell boundaries implies an overlapping with the Eulerian cells. It defines new sub-volumes with states corresponding to those of the Lagrangian cells. The number of sub-volumes per Eulerian cells ranges from 1 to 3. The conservative variables vector is updated with (1.7). The relaxation procedure (2.18), (2.19) is then used with the three sub-volumes and states for the pressure computation. The conservative and primitive variables vectors are now determined in the Eulerian cell. However, to proceed to the next time step, a specific procedure is needed.
- In order that the transformation from primitive to conservative variables be reversible and conservative the adiabatic exponent has to be modified:

$$\gamma_{\mathrm{num}} = \frac{p^* + \langle\rho\rangle\langle e\rangle}{\langle\rho\rangle\langle e\rangle - p_\infty(\langle\rho\rangle)}, \tag{3.7}$$

where p^* denotes the pressure obtained from the relaxation procedure (2.18), (2.19) and the symbol $\langle\cdot\rangle$ represents cell averages. Indeed, the relaxed pressure has to be equal to the one given by the true equation of state: $p = (\gamma - 1)\langle\rho\rangle\langle e\rangle - \gamma p_{\infty f}(\langle\rho\rangle)$.

- The numerical adiabatic exponent is convected during the Lagrange step. It means that the following equation is solved:

$$\frac{\mathrm{d}\gamma_{\mathrm{num}}}{\mathrm{d}t} = 0, \tag{3.8}$$

with initial conditions $\gamma_{\mathrm{num}} = \gamma$.

Corrections related to Eqs. (3.7), (3.8) are particularly important for the computation of the next time step. Consider for example the advection of a density discontinuity in uniform pressure and velocity fields. At the end of the first time step the conservative and primitive variables vectors are perfectly determined. The second Lagrangian step is now done. For this simple advection test, the waves incoming the Lagrangian cell have zero amplitude. Thus, the densities and internal energies of each sub-volume are equal to the Eulerian cell averaged ones of the first time step. Thus, the pressure in the Lagrangian cell is given by $p = (\gamma - 1)\rho_j e_j - \gamma p_{\infty f}(\rho_j) = (\gamma - 1)\langle\rho\rangle\langle e\rangle - \gamma p_{\infty f}(\langle\rho\rangle)$, where j denotes any sub-volume of the Lagrangian cell. This pressure is equal to the initial uniform pressure only if (3.8) is solved.

The need to define the numerical adiabatic exponent (3.7) and integration of (3.8) are consequences of the cell microstructure that is lost at the end of each time step.

3.4. Numerical example

The example of Fig. 3 with the Cochran–Chan EOS is again considered with the same conditions. This EOS can be expressed under Mie–Grüneisen form with $\gamma = 1 + \Gamma$ and $p_\infty(\rho) = \frac{1}{\gamma}(\rho\Gamma e_k(\rho) - p_k(\rho))$. We consider the

same advection problem as in Fig. 3. The results are shown at the same instant in Fig. 6. The same mesh is used.

It is clear that the new method improves the accuracy. However, its main drawback is related to its computational cost. The pressure is computed with the relaxation system (2.18), (2.19) solved by the Newton method. Such a procedure is very similar to an iterative Riemann solver, resulting in a significant computational cost. A simplified version of the algorithm is thus necessary.

4. A simplified relaxation method: the numerical EOS

The main difference with the Godunov method relies in relation (3.3):

$$p^* = \rho(\gamma - 1)\left\{E^0 - \frac{1}{2}u^{*^2}\right\} - \gamma \sum_j \beta_j^* p_{\infty j}(\rho_j^*).$$

The use of this equation of state requires computational efforts as the sub-volume fractions β_j^* and densities ρ_j^* at relaxed state are determined by the resolution of system (2.18), (2.19). The differences between the pressure computed with the Godunov method (3.4) and the present one (3.3) are arbitrarily large at contact discontinuities. But the contact discontinuity is also the place where the sub-volume fractions have the smallest variations, in particular during the projection stage. We propose to introduce minor changes in the algorithm presented in Section 3.3. The pressure is no longer computed by solving the nonlinear system (2.18), (2.19). At the end of the projection step the pressure is computed with the following numerical EOS:

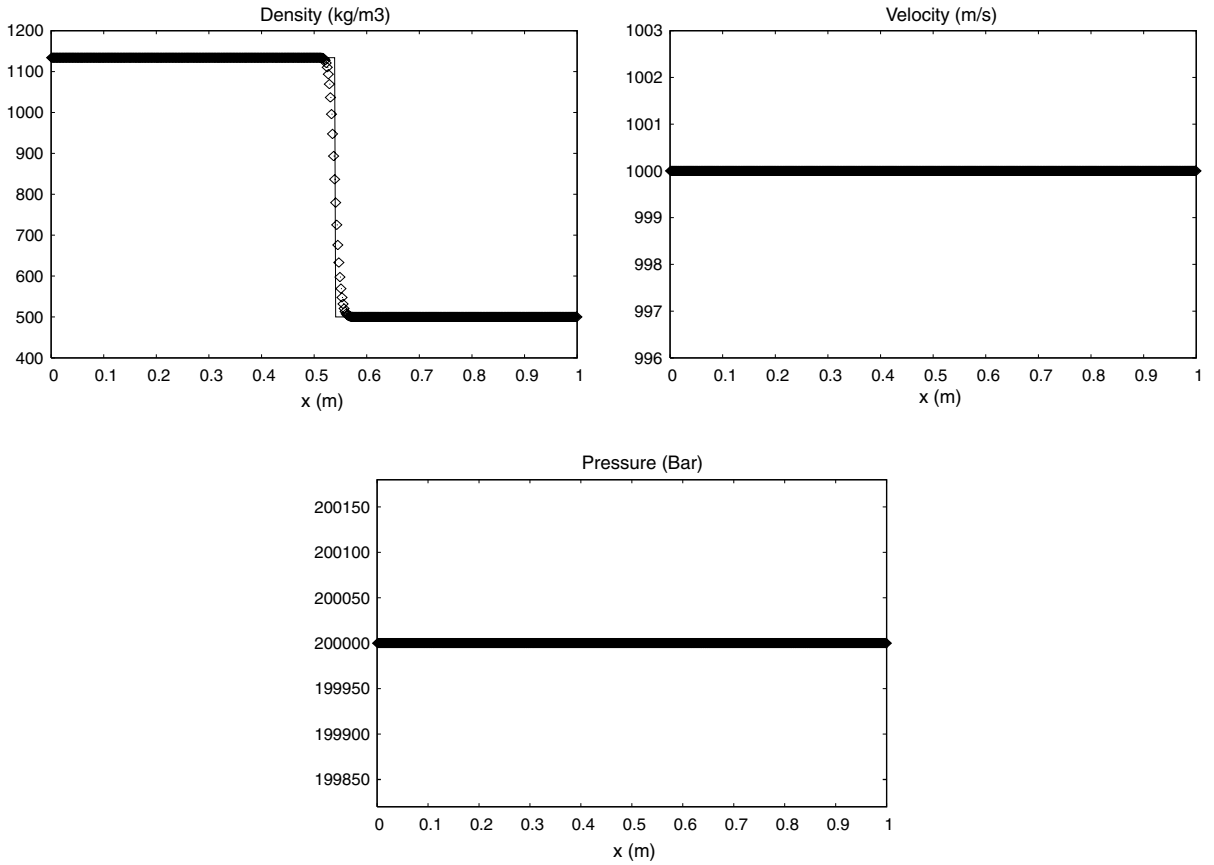

Fig. 6. Advection of a density discontinuity with the Cochran–Chan EOS. The solution obtained with the new relaxation method, based on (2.18), (2.19) is shown with symbols and the exact solution is shown with solid lines. Spurious oscillations are now cleared.

$$p^* = (\gamma - 1)\langle\rho\rangle\langle e\rangle - \gamma \sum_j \beta_j^0 p_{\infty j}(\rho_j^0) \tag{4.1}$$

with the cell averaged density $\langle\rho\rangle$ and internal energy $\langle e\rangle$ (this is not different of (3.3)). The sub-volume fractions β_j and densities ρ_j are taken equal to those of the Lagrangian cells. It means that frozen volume fractions are used and that variations due to pressure relaxation are neglected. Doing so, the method is much faster because iterative procedures are removed.

The accuracy of this method is now compared to the Godunov one, with exact Riemann solver. A shock tube problem involving liquid nitromethane (as in the previous numerical example) is considered. The coeffi-

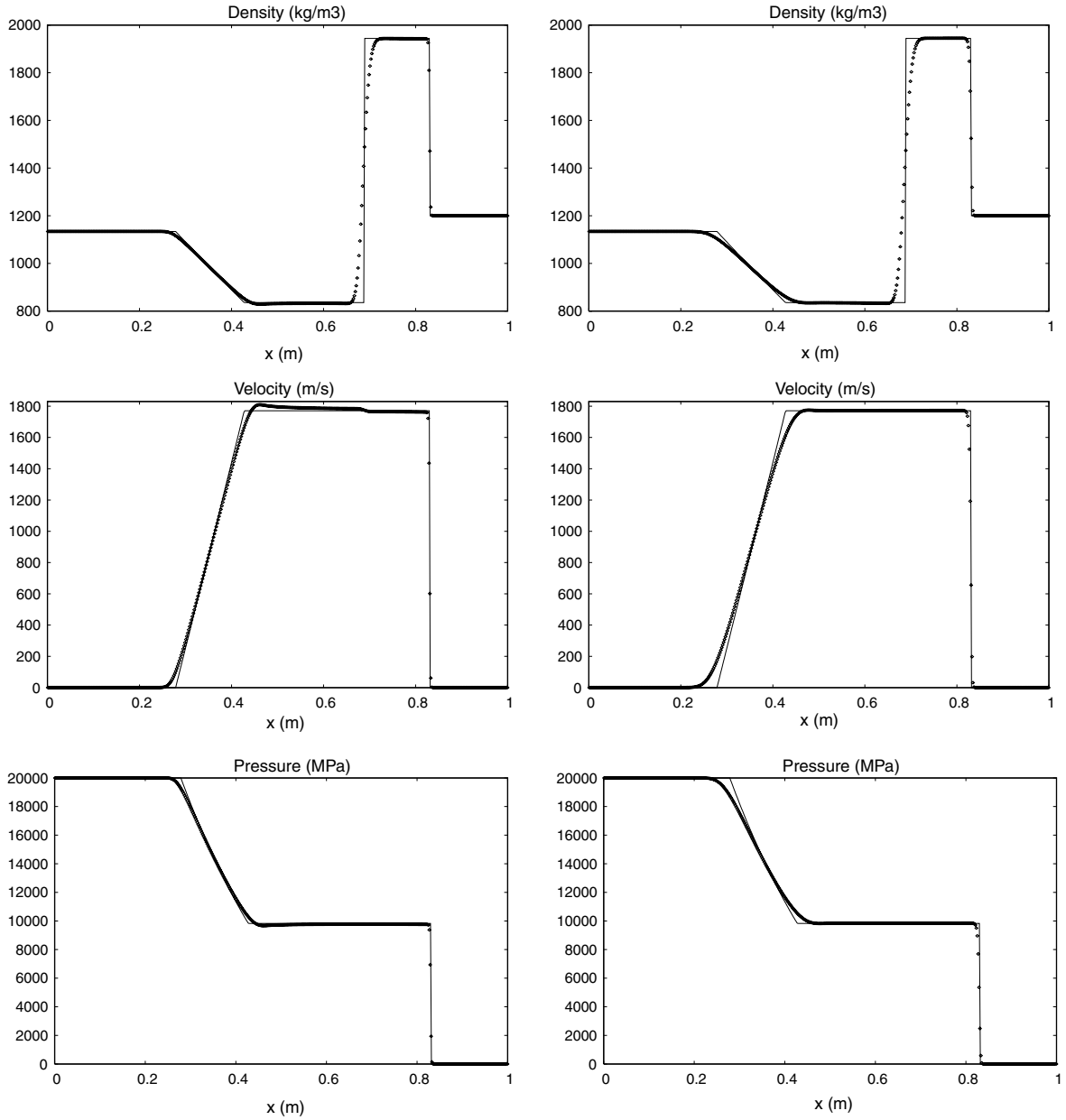

Fig. 7. Shock tube problem with Mie–Grüneisen EOS. The solution obtained with the Godunov scheme is shown on the left column with symbols. The solution obtained with the numerical EOS (4.1) is plotted in the right column with symbols. The exact solution is shown with solid lines. The new method is free of oscillations.

cients of the Cochran–Chan EOS are given in Section 1.3. At the initial time, the high pressure chamber is set to 2×10^{10} Pa, while the pressure is set equal to 2×10^5 Pa in the low pressure chamber. The fluid density in the high pressure chamber is set equal to 1134 kg/m^3 and to 1200 kg/m^3 in the low pressure chamber. The initial discontinuity is located at $x = 0.6$ m. The Godunov scheme and the new method are compared to the exact solution. In the new method, the numerical EOS (4.1) is used. The mesh involves 500 cells and the solutions are plotted in Fig. 7 at time $t = 50$ μs.

A magnified view of the velocity and pressure profiles is given in Fig. 8.

Clearly the numerical EOS (4.1) improves the computations and results in considerable computational time saving compared to System (2.18), (2.19).

5. The numerical EOS for interface problems

A variant of the preceding method can be developed for the computation of interfaces separating compressible fluids governed by different equations of state. Let us take the example of an interface separating a compressible liquid, governed by the stiffened gas EOS (1.2) with parameters γ_1 and $p_{\infty 1}$, and a gas governed by the same equation of state with parameters γ_2 and $p_{\infty 2}$. These EOS parameters are constant in each fluid, but are discontinuous at the interface.

Contrarily to the Mie–Grüneisen case, the adiabatic exponents are no longer constant and the numerical EOS now reads, from (3.1):

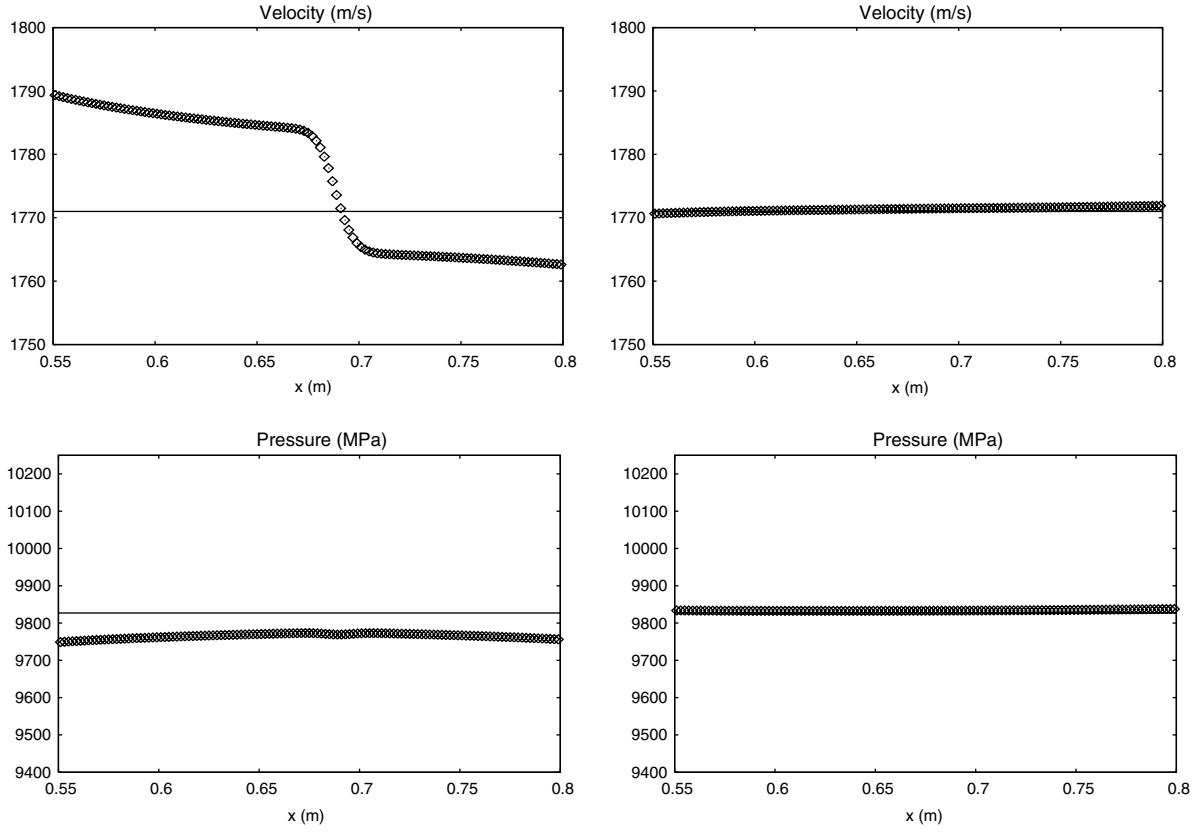

Fig. 8. Shock tube problem with Mie–Grüneisen EOS. A zoom of velocity and pressure profiles around the contact discontinuity is shown. Results obtained with the Godunov method are shown on the left column with symbols. The solution obtained with the new method is also shown with symbols in the right column. The exact solution is shown with lines.

$$p^* = \frac{\langle\rho\rangle\langle e\rangle - \sum_j \frac{\beta_j^0 \gamma_j p_{\infty j}}{\gamma_j - 1}}{\sum_j \frac{\beta_j^0}{\gamma_j - 1}}. \tag{5.1}$$

This relation is used to compute the pressure in Eulerian cells, at the end of the projection step. As previously with the Mie–Grüneisen EOS, the sub-volume fractions β_j are taken equal to those of the Lagrangian cells. It means that volume fraction variations due to pressure relaxation are again neglected. The numerical EOS allows the computation of numerical EOS parameters:

$$\begin{aligned} &\frac{1}{\gamma_{\text{num}} - 1} = \sum_j \frac{\beta_j^0}{\gamma_j - 1} \iff \gamma_{\text{num}} = 1 + \frac{1}{\sum_j \frac{\beta_j^0}{\gamma_j - 1}}, \\ &\gamma_{\text{num}} p_{\infty,\text{num}} = \frac{\sum_j \frac{\beta_j^0 \gamma_j p_{\infty j}}{\gamma_j - 1}}{\sum_j \frac{\beta_j^0}{\gamma_j - 1}} \iff p_{\infty,\text{num}} = \frac{\gamma_{\text{num}} - 1}{\gamma_{\text{num}}} \sum_j \frac{\beta_j^0 \gamma_j p_{\infty j}}{\gamma_j - 1}. \end{aligned} \tag{5.2}$$

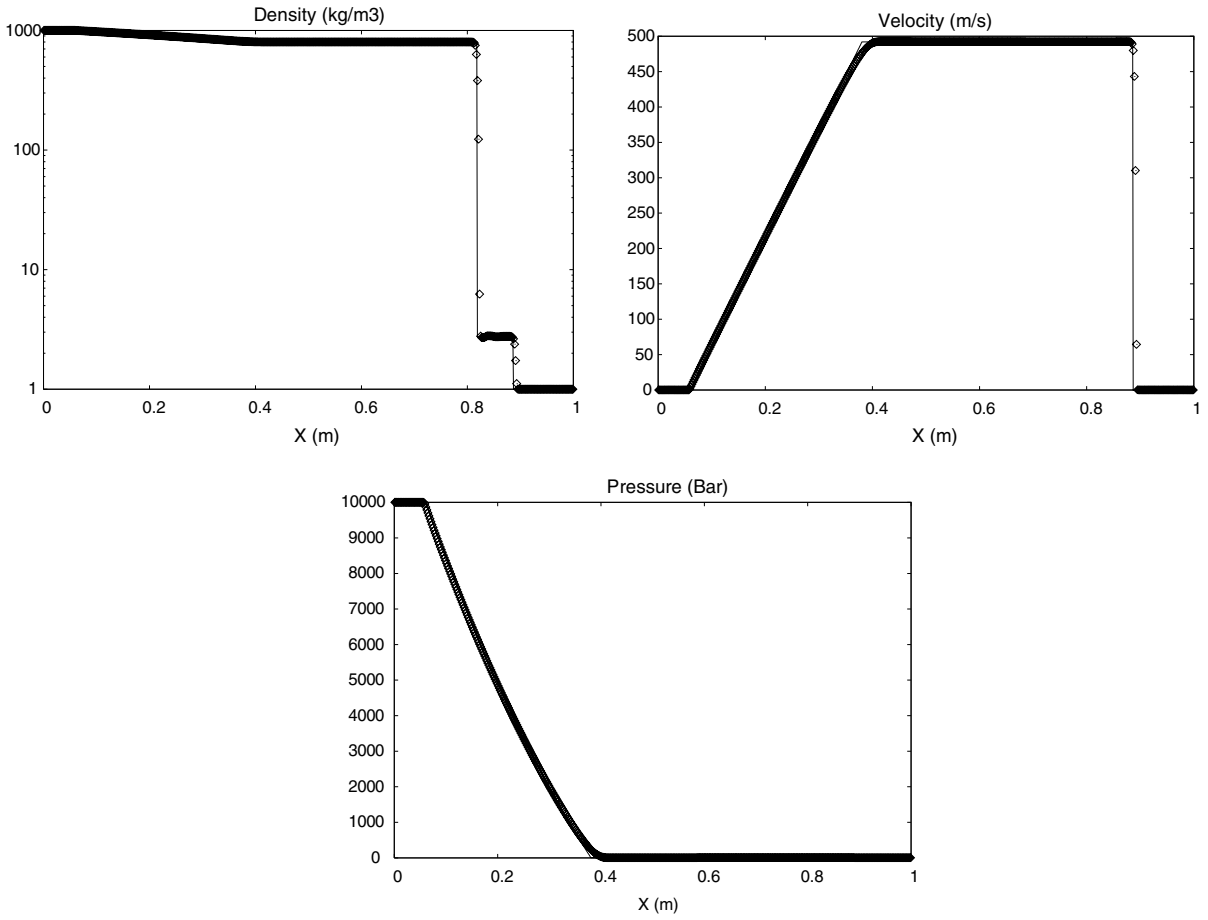

Fig. 9. Water–air shock tube problem. Comparison of the Lagrange-projection with Superbee limiter (symbols) and the exact solution (solid lines). A mesh involving 500 cells is used and the solution is shown at time $t = 241$ μs.

The numerical EOS parameters are then convected during the Lagrange step. It means that the following equations are solved:

$$\begin{aligned} \frac{\mathrm{d}\gamma_{\mathrm{num}}}{\mathrm{d}t} &= 0, \\ \frac{\mathrm{d}p_{\infty,\mathrm{num}}}{\mathrm{d}t} &= 0. \end{aligned} \tag{5.3}$$

This method is reminiscent of [15] method. There are however important differences:

- During the projection step, the update of γ_{num} and $p_{\infty,\mathrm{num}}$ with the help of (5.2) corresponds to the addition of a source term in Eq. (5.3).
- Also, when a shock interacts with an interface, there is the possibility to account for the sub-volumes fractions β_j variations. The pressure in the Eulerian cells is computed with the iterative version based on relations (2.18), (2.19). The numerical EOS parameters γ_{num}, $p_{\infty,\mathrm{num}}$ are computed with formulas (5.2) using relaxed state sub-volumes fractions β_j^* instead of β_j^0. The presence of a pressure wave inside the Eulerian cell is detected if $\mathrm{Max}_j(\frac{p_j - p_1}{p_1}) > 0.01$.

The method is illustrated on the following example. Let us consider a 1 m length shock tube, containing two chambers separated by an interface at location $x = 0.7$ m. The high pressure chamber on the left part is filled with liquid water ($\gamma_1 = 4.4$, $p_{\infty 1} = 6 \times 10^8$ Pa), the initial pressure is equal to 10^9 Pa and the initial density is equal to 1000 kg/m^3. The low pressure chamber on the right is filled with air ($\gamma_2 = 1.4$, $p_{\infty 2} = 0$ Pa), the initial pressure is equal to 10^5 Pa, and the density is equal to 1 kg/m^3. The fluid is initially at rest in both chambers. The solution is shown at time $t = 241$ μs. A mesh involving 500 cells is used.

The solution of the Lagrange-projection method with piecewise linear reconstruction and Superbee limiter in both Lagrange and projection steps is used. The second order extension of the present method is detailed in Appendix A. In Fig. 9, the density, pressure and velocity profiles are shown with symbols and compared to the exact solution with lines.

This test shows that the method is able to solve interface problems in the presence of strong shocks and very large density ratios.

6. Conclusion

A new relaxation-projection method has been built for the pressure computation when complex EOS are involved. The Godunov averages are not compatible with a direct use of the equation of state whose validity is restricted to local variables, not averaged ones. The new method determines the pressure as an asymptotic solution of a relaxation system involving the various sub-volumes present in a computational cell. These sub-volumes are associated to the propagation distances of the various waves coming from the cell boundaries. The method gives a cure to the pressure computation at contact discontinuities when complex EOS are used: real gases and discontinuous EOS. A simplified version is derived (the Numerical EOS) for the building of a fast algorithm.

Both methods (iterative and simplified) provide conservative and oscillation free results. They are validated against exact solutions of contact discontinuities with Mie–Grüneisen EOS and liquid–gas interfaces.

Its extension to the non-conservative multiphase flow model of Kapila et al. [8] is the aim of a companion paper [12].

Acknowledgments

This work was partially supported by DGA Centre d'Etudes de Gramat. The authors are particularly grateful to Dr. Gérard Baudin. They also address special thanks to the Associate Editor and Referees for important remarks and suggestions.

Appendix A. Second order extension of the numerical EOS method for interface problems

The results of Section 5 are obtained with the following second order extension of the method. The strategy follows the lines of the MUSCL algorithm [21,22]. However the presence of an interface necessitates specific ingredients as detailed hereafter:

- Second order Lagrange step
  - The conservative variables vector U is evolved during a half-time step in the Lagrangian cell, with the help of Formula (1.5).
  - The primitive variables $W=(\rho,u,p)^{\mathrm{T}}$ slopes $\delta W_i=\frac{W_{i+1}^{n+1/2}-W_i^{n+1/2}}{x_{i+1}^{n+1/2}-x_i^{n+1/2}}$ are computed in each cell. The cell center positions are obtained from the cell boundary positions, updated with (1.3): $x_i^{n+1/2}=\frac{x_{i+1/2}^{n+1/2}+x_{i-1/2}^{n+1/2}}{2}$.
  - A slope limiter is used : $\delta\overline{W}_i=\Phi(\delta W_{i-1},\delta W_i)$, where Φ denotes an appropriate limiter function (Minmod, Superbee, etc.).
  - The primitive variable vector is extrapolated from the cell center to the cell boundaries by using the preceding limited gradients.
  - The Riemann problem is solved and the Lagrangian flux is computed.
  - The conservative variable vector is evolved over a complete time step with formula (1.5) with the preceding Lagrangian flux.
  - The pressure is computed with: $p_i^{n+1}=(\gamma_{\mathrm{num},i}^{n+1}-1)(\rho e)_i^{n+1}-\gamma_{\mathrm{num},i}^{n+1}p_{\infty\mathrm{num},i}^{n+1}$; Where the integration of (5.3) reduces to: $\gamma_{\mathrm{num},i}^{n+1}=\gamma_{\mathrm{num},i}^{n}$ and $p_{\infty\mathrm{num},i}^{n+1}=p_{\infty\mathrm{num},i}^{n}$.
- Second order projection step
  - The density and numerical EOS parameters gradients are computed:

$$\delta\rho_i=\frac{\rho_{\mathrm{L},i+1}^{n+1}-\rho_{\mathrm{L},i}^{n+1}}{x_{i+1}^{n+1}-x_i^{n+1}},$$

$$\delta\left(\frac{1}{\gamma_{\mathrm{num}}-1}\right)_i=\frac{\left(\frac{1}{\gamma_{\mathrm{num}}-1}\right)_{\mathrm{L},i+1}^{n+1}-\left(\frac{1}{\gamma_{\mathrm{num}}-1}\right)_{\mathrm{L},i}^{n+1}}{x_{i+1}^{n+1}-x_i^{n+1}},$$

$$\delta\left(\frac{\gamma_{\mathrm{num}}p_{\infty,\mathrm{num}}}{\gamma_{\mathrm{num}}-1}\right)_i=\frac{\left(\frac{\gamma_{\mathrm{num}}p_{\infty,\mathrm{num}}}{\gamma_{\mathrm{num}}-1}\right)_{\mathrm{L},i+1}^{n+1}-\left(\frac{\gamma_{\mathrm{num}}p_{\infty,\mathrm{num}}}{\gamma_{\mathrm{num}}-1}\right)_{\mathrm{L},i}^{n+1}}{x_{i+1}^{n+1}-x_i^{n+1}},$$

  where the subscript L denotes the variables in Lagrangian cells.
  - These gradients are limited as previously during the Lagrangian step.
  - In order to avoid spurious pressure and velocity oscillations, the momentum and total energy gradients are computed by:

$$\delta\overline{\rho u}_i=u_{\mathrm{L},i}^{n+1}\delta\overline{\rho}_i,$$

$$\delta\overline{\rho E}_i=p_{\mathrm{L},i}^{n+1}\delta\left(\overline{\frac{1}{\gamma_{\mathrm{num}}-1}}\right)_i+\delta\left(\overline{\frac{\gamma_{\mathrm{num}}p_{\infty,\mathrm{num}}}{\gamma_{\mathrm{num}}-1}}\right)_i+\frac{(u_{\mathrm{L},i}^{n+1})^2}{2}\delta\overline{\rho}_i,$$

  where the pressure and velocity gradients are forced to vanish.
  - The sub-volume fraction β_j appearing in Formula (1.7) is computed.
  - The piecewise linear conservative variables vector is averaged over each sub-volume present in the Eulerian cell in order to determine U_j^{n+1}.
  - The conservative variables are averaged with the help of (1.7).
  - The cell pressure is computed by (5.1) and the numerical EOS parameters by (5.2).

References

[1] R. Abgrall, How to prevent pressure oscillations in multicomponent flow calculations: a quasi conservative approach, J. Comput. Phys. 125 (1996) 150–160.
[2] R. Abgrall, R. Saurel, Discrete equations for physical and numerical multiphase mixtures, J. Comput. Phys. 186 (2) (2003) 361–396.
[3] G. Cochran, J. Chan, Shock initiation and detonation models in one and two dimensions, CID-18024 Lawrence National Laboratory Report, 1979.
[4] A. Chinnayya, E. Daniel, R. Saurel, Computation of detonation waves in heterogeneous energetic materials, J. Comput. Phys. 196 (2004) 490–538.
[5] S.F. Davis, Simplified second-order Godunov-type methods, SIAM J. Sci. Stat. Comput. 9 (1988) 445–473.
[6] S.K. Godunov, A. Zabrodin, M. Ivanov, A. Kraiko, G. Prokopov, in: Mir (Ed.) Résolution numérique des problèmes multidimensionnels de la dynamique des gaz, Moscow, 1979 (in French).
[7] A. Harten, P.D. Lax, B. van Leer, On upstream differencing and Godunov-type schemes for hyperbolic conservation laws, SIAM Rev. 25 (1) (1983) 35–61.
[8] A.K. Kapila, Menikoff, J.B. Bdzil, S.F. Son, D.S. Stewart, Two-phase modeling of deflagration to detonation transition in granular materials: reduced equations, Phys. Fluids 13 (10) (2001) 3002–3024.
[9] S. Karni, Multicomponent flow calculation by a consistent primitive algorithm, J. Comput. Phys. 112 (1994) 31–43.
[10] O. Le Metayer, J. Massoni, R. Saurel, Modelling evaporation fronts with reactive Riemann solvers, J. Comput. Phys. 205 (2005) 567–610.
[11] R. Liska, B. Wendroff, Comparison of several difference schemes on 1D and 2D test problems for the Euler equations, SIAM J. Sci. Comput. 25 (2003) 995–1017.
[12] F. Petitpas, E. Franquet, R. Saurel, A relaxation-projection method for compressible flows. Part II: computation of interfaces and multiphase mixtures with stiff mechanical relaxation. J. Comput. Phys. (submitted for publication).
[13] R. Saurel, M. Larini, J.C. Loraud, Exact and approximate Riemann solvers for real gases, J. Comput. Phys. 112 (1) (1994) 126–137.
[14] R. Saurel, R. Abgrall, A multiphase Godunov method for compressible multifluid and multiphase flows, J. Comput. Phys. 150 (1999) 425–467.
[15] R. Saurel, R. Abgrall, A simple method for compressible multifluid flows, SIAM J. Sci. Comput. 21 (3) (1999) 1115–1145.
[16] R. Saurel, O. Le Metayer, A multiphase model for interfaces, shocks, detonation waves and cavitation, J. Fluid Mech. 431 (2001) 239–271.
[17] R. Saurel, S. Gavrilyuk, F. Renaud, A multiphase model with internal degree of freedom: application to shock-bubble interaction, J. Fluid Mech. 495 (2003) 283–321.
[18] E.F. Toro, Some IVPs for which conservative methods fail miserably, in: Proceedings of the 6th International Symposium on Computational Fluid Dynamics, Lake Tahoe, Nevada, USA, September 4–8, 1995.
[19] E.F. Toro, Riemann Solvers and Numerical Methods for Fluids Dynamics, Springer, Berlin, 1997.
[20] E.F. Toro, Anomalies of conservative methods: analysis, numerical evidence and possible cures, Comput. Fluid Dyn. J. 11 (2) (2002) 128–143.
[21] B. Van Leer, Towards the ultimate conservative difference scheme IV. A new approach to numerical convection, J. Comput. Phys. 23 (1977) 276–299.
[22] B. Van Leer, Towards the ultimate conservative difference scheme V. A second order sequel to Godunov's method, J. Comput. Phys. 32 (1979) 101–136.